ARTICLE   OPEN

Check for updates

Constrained tropical land temperature-precipitation sensitivity reveals decreasing evapotranspiration and faster vegetation greening in CMIP6 projections

Boyuan Zhu[1,2], Yongzhou Cheng[1,2], Xuyue Hu[1,2], Yuanfang Chai [ID][3 ✉], Wouter R. Berghuijs[4], Alistair G. L. Borthwick [ID][5,6] and Louise Slater [ID][7]

Over the tropical land surface, accurate estimates of future changes in temperature, precipitation and evapotranspiration are crucial for ecological sustainability, but remain highly uncertain. Here we develop a series of emergent constraints (ECs) by using historical and future outputs from the Coupled Model Inter-comparison Project Phase 6 (CMIP6) Earth System Models under the four basic Shared Socio-economic Pathway scenarios (SSP126, SSP245, SSP370, and SSP585). Results show that the temperature sensitivity to precipitation during 2015–2100, which varies substantially in the original CMIP6 outputs, becomes systematically negative across SSPs after application of the EC, with absolute values between $-1.10\,°C\,mm^{-1}$ day and $-3.52\,°C\,mm^{-1}$ day, and with uncertainties reduced by 9.4% to 41.4%. The trend in tropical land-surface evapotranspiration, which was increasing by $0.292\,mm\,yr^{-1}$ in the original CMIP6 model outputs, becomes significantly negative ($-0.469\,mm\,yr^{-1}$) after applying the constraint. Moreover, we find a significant increase of 58.7% in the leaf area index growth rate.

INTRODUCTION

Over the tropical land surface, a negative association between temperature and precipitation is generally observed due to the cooling effect of land surface evapotranspiration, and is one of the major processes between the earth and the atmosphere[1–3]. However, future changes in these variables under climate change remain highly uncertain. Thus, a robust evaluation of future changes in temperature-precipitation-evapotranspiration and their interaction is necessary to assess the potential resilience of tropical land areas to future climate change.

Previous studies have investigated current and future temperature, precipitation, and evapotranspiration changes from regional to global scales, using Earth System Models from the CMIP5 ensemble[4–8]. These studies were based on analyses of thermodynamic and dynamic responses to changes in variables such as specific humidity and atmospheric circulation. Although the models accommodate important processes, such as convection, aerosol effects, and land–atmosphere and dynamic ocean–atmosphere interactions, the results show considerable spread[9]. The emergent constraint (EC) method has recently been employed to reduce uncertainty in the model outputs, and has led to significant improvement[10–13]. The constraint is typically built through a physically explainable empirical linear regression between the inter-model spread in future estimates of temperature/precipitation/evapotranspiration (i.e. their absolute value or their sensitivity to controlling factors, defined as the dependent variable y) and historical values of variables (defined as the independent variable x) produced by the CMIP5 ensemble[10,11]. This relation can then be further constrained by projecting observed values of x and their observational uncertainty (± one

standard deviation, denoted as SD) onto the y-axis through the empirical linear relationship[10,11], as the observed values are likely to be sufficiently reliable to provide an accurate mean state of x. This approach provides more reliable values of y with expectably narrower uncertainty[10–12].

CMIP6, the latest generation of CMIP, has finer horizontal-vertical resolutions and more physically realistic representations of aerosol, cloud-radiation interaction, oceanic horizontal-vertical mixing and convection, sea ice, and biogeochemical processes (e.g. carbon and nitrogen cycles) than its predecessor, CMIP5[10,14]. Recent works concerned with reproducing historical changes and predicting future features in global temperature, precipitation, and evapotranspiration have demonstrated that CMIP6 models provide projections that are more accurate and reliable than their CMIP5 counterparts[15–17].

Despite these improvements in CMIP6, there remains considerable uncertainty in the projections of the sensitivity of future surface temperature to precipitation over the tropical land surface, and the future growth rate of evapotranspiration and vegetation cover. CMIP models (and constrained projections using the EC method) have projected a decline of the tropical forest, especially in the Amazon, but the projection accuracy depends largely on the reliability of the environmental variable projections[12,18–23]. The tropical forest cover is closely related to factors such as temperature, precipitation and evapotranspiration. As temperatures rise, the rates of plant transpiration and respiration grow significantly due to amplified vegetation stomatal openings. This intensification leads to substantial losses of water and CO_2 within plant bodies, subsequently causing notable constraints in water use efficiency, photosynthesis and CO_2 fertilization which

[1]School of Hydraulic and Environmental Engineering, Changsha University of Science & Technology, Changsha 410114, China. [2]Key Laboratory of Water-Sediment Sciences and Water Disaster Prevention of Hunan Province, Changsha 410114, China. [3]State Key Laboratory of Earth Surface Processes and Resource Ecology, Faculty of Geographical Science, Beijing Normal University, Beijing 100875, China. [4]Department of Earth Sciences, Free University Amsterdam, Amsterdam 1081 HV, the Netherlands. [5]School of Engineering, The University of Edinburgh, Edinburgh EH9 3JL, UK. [6]School of Engineering, Computing and Mathematics, University of Plymouth, Plymouth PL4 8AA, UK. [7]School of Geography and the Environment, University of Oxford, Oxford OX1 3QY, UK. ✉email: yuanfangchai@163.com

ultimately suppress plant growth[12,18–24]. Under decreasing precipitation, lower water availability is also unfavorable for plant growth[12,18–20,22–24].

Here we assess the reliability of future projections of tropical land-surface temperature-precipitation sensitivity, evapotranspiration and leaf area index (LAI). We first explore the sensitivity of temperature to precipitation over the tropical land area within 23.5°S–23.5°N and 180° W–180°E. Our methodology is based on an emergent relationship established between the future annual tropical land-surface temperature sensitivity to precipitation (dT/dP) and the historical seasonal average dT/dP under the four basic SSP scenarios of CMIP6. The projected changes in tropical land-surface temperature sensitivity are then employed to estimate absolute variations in future tropical land-surface temperature, evapotranspiration and LAI.

RESULTS

Sensitivity of tropical land-surface temperature to precipitation

It is widely acknowledged that the increasing atmospheric CO_2 concentration is the main driving factor behind the significant warming of the Earth's surface[25–28]. However, interannual oscillations in temperature may also be related to local precipitation changes, which has been identified in the Amazon rainforest[12]. Observed time series of annual land-surface temperature and precipitation in the tropical zone from the HadCRUT4 dataset display oscillations roughly in antiphase during the period of 1949 to 2005 (Fig. 1a). Negative associations are found at the annual and seasonal scale between land-surface temperature and precipitation anomalies (Fig. 1b). Supportive results are also derived from three other datasets (Supplementary Figs. 1, 2).

The underlying mechanism of the negative sensitivity of tropical land-surface temperature to precipitation (i.e. opposite oscillations in Fig. 1a and Supplementary Fig. 1) is as follows: increasing precipitation leads to more water availability in the soil and on the ground, enhancing the cooling effect of evapotranspiration on sensible heating, and subsequently lowering the temperature of the tropical land surface[1,2,29]. This interpretation is supported by antiphase oscillations between annual mean evapotranspiration and temperature on the tropical land surface (Fig. 1c and Supplementary Fig. 3). Recent research also revealed that water availability (and especially extreme drought) affects fluctuations of land-surface temperature in the tropical region, through vegetation stomatal responses to the soil-moisture-deficit induced atmospheric water stress or the plant metabolism downregulation[30]. Moreover, as the dominant extreme climate event in controlling matter-energy cycles between land surface and atmosphere over the tropical region, ENSO triggers subsidence/rising weather systems and subsequently causes concurrent warming (cooling), decreased (increased) humidity, less (more) cloud cover, less (more) precipitation, lower (higher) evaporation and less (more) soil moisture[2,31,32], strengthening the negative feedback between tropical land-surface temperature and precipitation. Here, if we use a moving average approach to reduce disturbance from climate oscillations (i.e. ENSO and other compensating effects)[9,31–33], we find that the negative association between temperature and precipitation is further strengthened (Fig. 1d, Supplementary Fig. 4 and Supplementary Fig. 5).

An effective index for representing tropical land-surface temperature change due to evapotranspiration arising from precipitation is the temperature sensitivity to precipitation (dT/dP, °C mm^{-1} day). We select a total of 26 models under the four SSP scenarios from the CMIP6 ensemble, which provide both the required historical (1949–2005) and future (2015–2100) temperature/precipitation outputs (Supplementary Table 1). A large spread occurs in the CMIP6 scenario estimates of the

absolute value of future annual dT/dP, as indicated by its considerable variability, ranging from −1.52 to 1.06 °C mm^{-1} day for SSP126, from −1.52 to 2.19 °C mm^{-1} day for SSP245, from −3.63 to 4.75 °C mm^{-1} day for SSP370, and from −4.31 to 5.00 °C mm^{-1} day for SSP585 (Fig. 1e). Since the feedback among temperature, precipitation and evapotranspiration is a key process between the land surface and the atmosphere, such large uncertainties may lead to comparable uncertainties in the cycle among water, carbon and energy on the tropical land[12].

Using evapotranspiration data from the GLEAM dataset during the period of 1980–2014, we calculated the annual rates of increase in evapotranspiration from the tropical land surface in wet and dry seasons (Jan. to Mar. and May to Jul., respectively), and found that the rate of increase was significantly larger in the dry season than in the wet season (0.23% yr^{-1} vs. 0.11% yr^{-1}, Supplementary Fig. 6). This difference is likely to be related to the seasonal effect of absolute water storage in the tropical land: in the wet season, water storage is large and reaches the upper limit of evapotranspiration, meaning that evapotranspiration cannot increase appreciably as water storage continues to increase; whereas in the dry season, water storage is scarce, and evapotranspiration is markedly enhanced as the water storage increases[34]. In summary, larger fluctuations in the evapotranspiration-cooling effect occur in the dry season, which profoundly affects the oscillation in tropical land-surface temperature. Observations show that the dry-season land-surface temperature exhibits tighter negative correlation (i.e. higher absolute values of R) with precipitation than the wet-season temperature (Fig. 1b, Supplementary Fig. 2), implying that changes in dry-season dT/dP values dominate the annual negative sensitivity of temperature to precipitation. Model results reveal that the future annual dT/dP exhibits a high positive correlation with the future dry-season dT/dP for all four emission scenarios ($0.49 \leq R \leq 0.81$, $P < 0.001$, Fig. 1f), suggesting that the spread in future dry-season dT/dP (Supplementary Fig. 7) will lead to a comparable spread in future annual dT/dP. Therefore, we can expect to constrain the future annual dT/dP through establishing an emergent relationship between the future annual dT/dP and the historical dry-season dT/dP. In fact, a similar emergent constraint on future dT/dP has been identified in the Amazon rainforest[12].

EC on future dT/dP based on the CMIP6 ensemble

We observed significant linear regressions (along with their corresponding errors) between the future annual and the historical dry-season average values of dT/dP for the four SSP scenarios (Fig. 2, Supplementary Fig. 8), based on the spread in the CMIP6 ensemble (Fig. 1e–f). Linear regressions between future annual and historical wet-season average values of dT/dP have lower values of R and higher P values (Supplementary Fig. 9), and therefore are not used. The observed dry-season average dT/dP (vertical black line) ± one standard deviation (light blue rectangle) derived from the HadCRUT4 dataset are then plotted for the four SSP scenarios (Fig. 2, Supplementary Fig. 8). These two steps together establish the ECs on future annual dT/dP for the four SSP scenarios. Associated probability density functions (PDFs) after applying the ECs are then calculated based on error intervals of both the observed historical dry-season average values and projected future annual values of dT/dP, while PDFs without the ECs are directly obtained from the CMIP6 ensemble (Fig. 2, Supplementary Fig. 8).

After the application of the ECs, the spreads of the PDFs under the four SSP scenarios become compressed, revealing large reductions in uncertainty in future annual dT/dP compared with the values directly derived from the CMIP6 ensemble. The reductions are 9.4%, 16.1%, 29.8%, and 41.4% for the four SSPs, respectively (Fig. 2, Supplementary Fig. 8). Importantly, the best
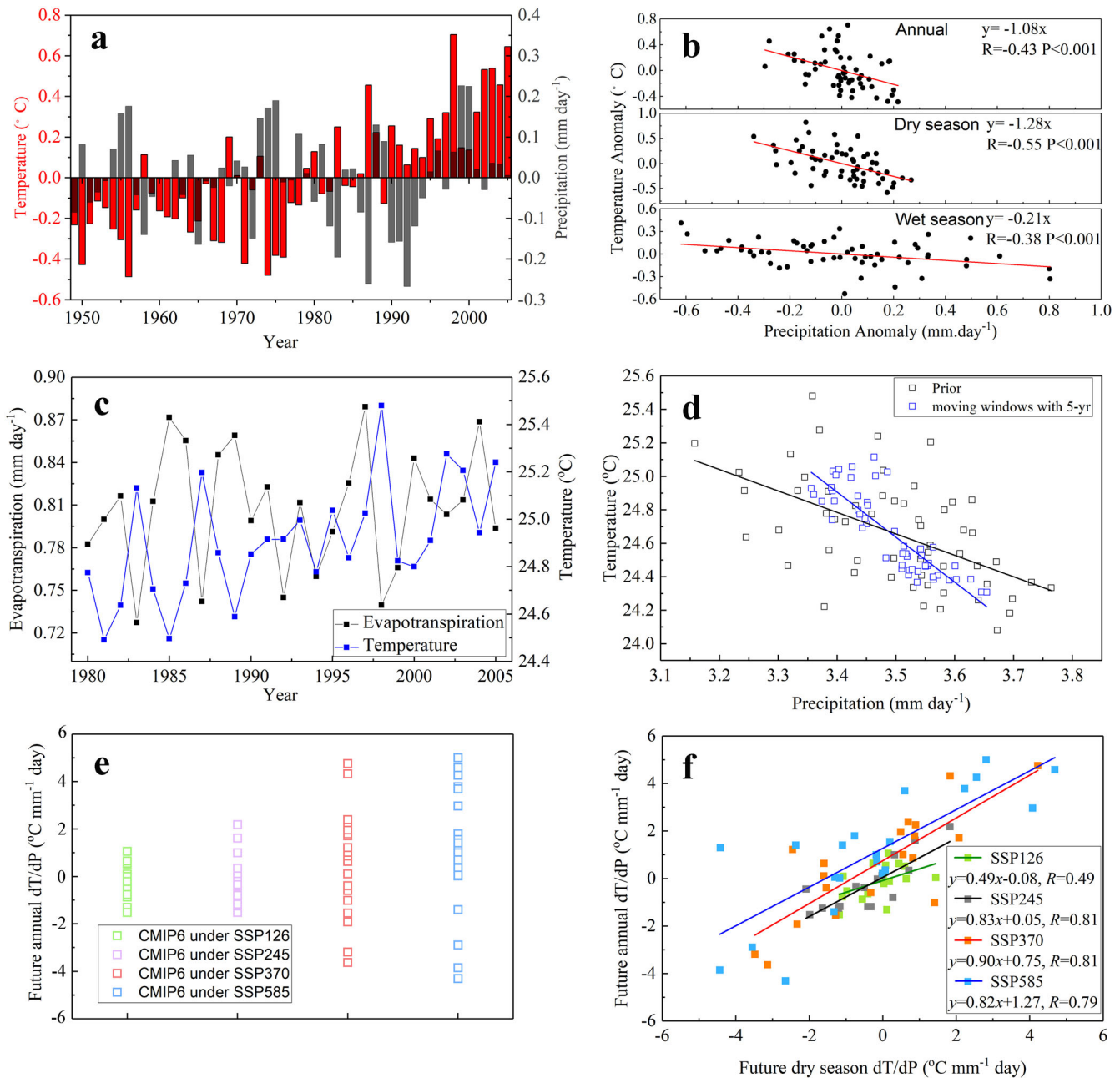
Fig. 1 Association between tropical land-surface temperature and precipitation using HadCRUT4 observations and CMIP6 outputs. **a** Observed time series of annual tropical land-surface temperature and precipitation from 1949 to 2005. **b** Observed relationship between tropical land-surface temperature and precipitation anomalies at annual and seasonal timescales (anomalies are computed as the value of a variable in a certain year minus the mean over the multi-year period of 1949–2005). **c** Comparison between the two observed yearly time series of tropical land-surface evapotranspiration from GLEAM dataset and temperature from HadCRUT4 dataset during 1980–2005. **d** Linear relationships between observed tropical land-surface temperature and precipitation before and after using a moving average with the window length of 5 years. Linear relationships corresponding to other window lengths are illustrated in Supplementary Fig. 4, and correlation coefficients and slope values (i.e., dT/dP) are provided in Supplementary Fig. 5. **e** Spreads of future annual dT/dP modeled under the four SSP scenarios. **f** Relationship between future annual and historical dry-season values of tropical land dT/dP modeled under the four SSP scenarios.

estimates of the constrained future annual dT/dP (each corresponding to the peak in the PDF) exhibit large decreases from pre-EC to post-EC conditions (Fig. 2, Supplementary Fig. 8, Supplementary Table 2). Pre-EC values of the best estimates of dT/dP are −0.14 °C mm^{-1} day, −0.27 °C mm^{-1} day, 0.57 °C mm^{-1} day, and 1.03 °C mm^{-1} day, respectively, under the four SSP scenarios (Fig. 2, Supplementary Fig. 8, Supplementary Table 2), suggesting uncertainty even in the sign of future annual dT/dP, if different SSP scenarios are used. However, the post-EC values drop to −1.10 °C

mm^{-1} day, −1.63 °C mm^{-1} day, −2.86 °C mm^{-1} day, and −3.52 °C mm^{-1} day, respectively, with the absolute decreases reaching 0.96 °C mm^{-1} day, 1.36 °C mm^{-1} day, 3.43 °C mm^{-1} day, and 4.55 °C mm^{-1} day, correspondingly (Fig. 2, Supplementary Fig. 8, Supplementary Table 2), meaning that future annual dT/dP becomes systematically negative across all SSP scenarios. Decreases from pre-EC to post-EC conditions are therefore conspicuous. PDFs based on the three other observational
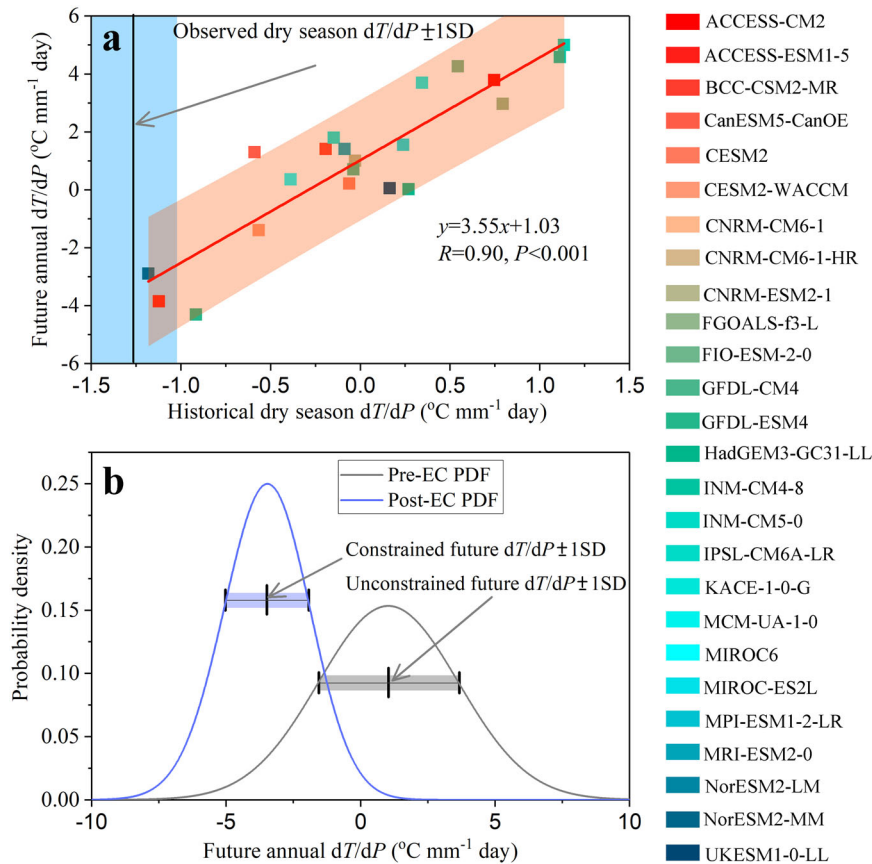
Fig. 2   EC on future annual dT/dP based on CMIP6 models under the SSP585 scenario. a The constraint consists of a linear regression (with the associated error) between the future annual simulated dT/dP and historical dry season simulated dT/dP (red line and orange shaded area); then the constrained data is computed by projecting the observed historical dry season dT/dP ± one standard deviation (vertical black line and light blue rectangle, obtained from the HadCRUT4 dataset) onto the regression. **b** Blue and gray lines are PDFs for the constrained (post-EC) and unconstrained (pre-EC) future annual dT/dP, showing the change in projection uncertainty and the best estimate of future annual dT/dP.

datasets also demonstrate reductions in both the uncertainty and the best estimate (Supplementary Fig. 10).

Out-of-sample testing is an effective way to assess whether these emergent relationships have emerged solely by chance[10]. Using 25 CMIP5 models, we still find a tight relationship between future annual dT/dP and historical dry-season dT/dP under the RCP2.6 scenario ($R = 0.64$, $P < 0.001$, Supplementary Fig. 11). When driving the relationship with the observations, the constraint also shifts the future annual dT/dP from $-0.89 \pm 0.79\,°C\,mm^{-1}$ day to a more negative value of $-1.43 \pm 0.65\,°C\,mm^{-1}$ day. This testing further supports the reliability of our introduced emergent constraint.

Future evapotranspiration from tropical land

Evapotranspiration from tropical land depends strongly on variations in tropical land temperature and precipitation, as is illustrated by the strong positive correlation between the future annual growth rate in evapotranspiration and the future annual dT/dP under the high emission scenario of SSP585 (Fig. 3a). By projecting the post-EC value of future annual dT/dP ± one standard deviation (vertical black line ± light blue rectangle) onto the y-axis through the linear regression relation (with forecast error), we find that evapotranspiration is likely to experience a reduction at a rate of $-0.469 \pm 0.430\,mm\,yr^{-1}$ under SSP585 during 2015–2100 (Fig. 3a). Conversely, under pre-EC conditions, an increasing rate of evapotranspiration of $0.292 \pm 0.533\,mm\,yr^{-1}$ is projected, corresponding to the peak of the pre-EC PDF curve (Fig. 3b). In other words, after application of the EC, evapotranspiration from tropical land is projected to decrease substantially

in the future under the high emission scenario of SSP585. Moreover, the PDF curve corresponding to the future annual trend in tropical land evapotranspiration shows a notable narrowing from pre-EC to post-EC conditions, suggesting a reduction of 19.3% in the uncertainty of the projection (Fig. 3b).

Past research suggests a significant decline in soil water content in the tropics accompanied by an expected rise in aridification[35]. This would result in the soil's water supply becoming inadequate to meet the increasing evaporative demand from the atmosphere. This may be the reason for the decrease in future tropical evapotranspiration. A similar feedback between soil water and evapotranspiration has been reported which suggested that the observed decline of global evapotranspiration during 1998-2008 was primarily driven by moisture shortage in the Southern Hemisphere[36].

Future vegetation greening on tropical land

Temperature and precipitation are key climatic factors that affect vegetation dynamics on the tropical land, as is confirmed by the strong relationship between the future annual growth rate in tropical land LAI and future annual dT/dP across CMIP6 models under the SSP585 scenario ($R = -0.82$, $P < 0.001$, Fig. 4a). The relationship indicates that a more negative dT/dP (i.e., a higher evaporative cooling effect) after application of the EC is associated with greater greening of tropical vegetation. Hence, the overestimate of future dT/dP by the original CMIP6 models implies that they equally underestimated the increase in tropical land vegetation. The original CMIP6 models projected a future annual
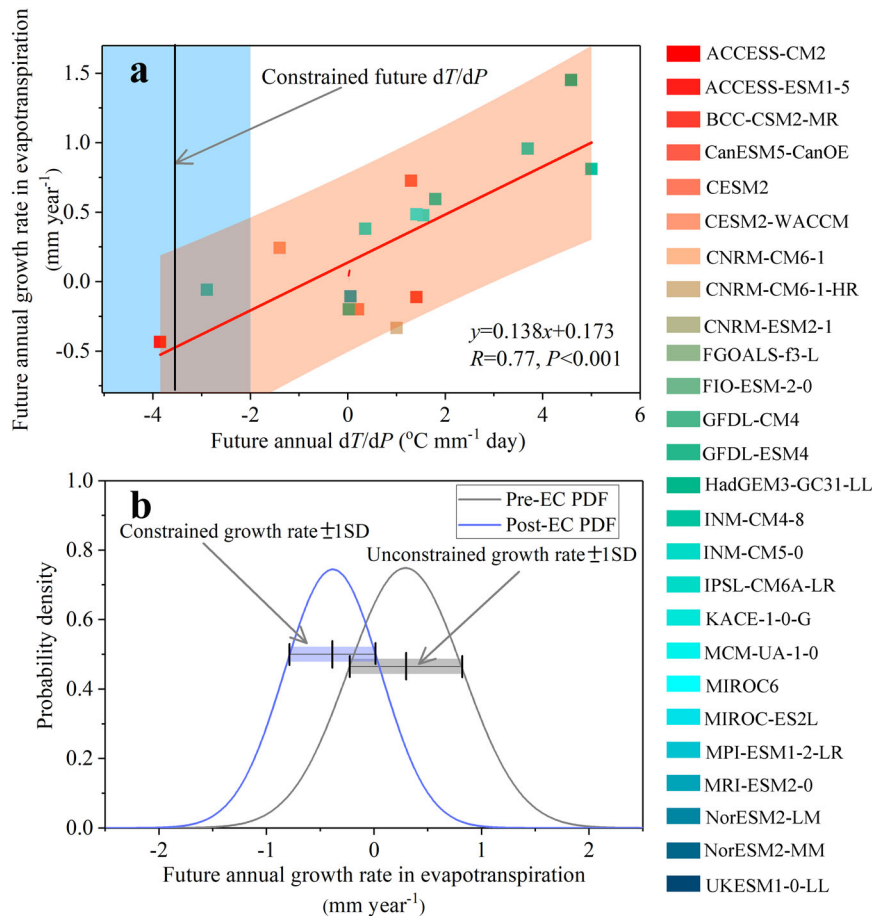
Fig. 3 EC on future annual growth rate in tropical land evapotranspiration based on CMIP6 models (see Supplementary Table 1) under the SSP585 scenario. a The constraint consists of a linear regression (with the associated forecast error) between the future annual dT/dP and future annual growth rate in evapotranspiration (red line and orange shaded area); the constrained data is computed by projecting the constrained future annual dT/dP ± one standard deviation (SD, vertical black line ± light blue rectangle) onto the regression. **b** Blue and gray lines are PDFs for the constrained (post-EC) and unconstrained (pre-EC) future annual growth rates in evapotranspiration. Note: The use of a constrained future variable (x) to constrain another future variable (y) has also been applied in previous studies[11,45]. The logic is as follows: A tight interdependence (i.e. emergent relationship) is first found between x and y based on originally modeled results. The constrained x is then applied in the emergent relationship to obtain a more precise y given that this kind of x shows a much lower uncertainty.

growth rate in LAI of 0.0085 ± 0.0073 m^2 m^{-2} yr^{-1} under the SSP585 scenario (Fig. 4b). However, after applying the constraint (Fig. 4a), the future tropical land LAI is expected to increase by 0.0205 ± 0.0065 m^2 m^{-2} yr^{-1}, demonstrating that the raw CMIP6 models underestimated the future increasing trend in tropical land LAI by 58.7% under the SSP585 scenario (Fig. 4b).

When there is enough water in the soil to meet the transpiration demand, the increase in the LAI growth rate typically strengthens the process of transpiration, and results in higher evapotranspiration. The counterintuitive downward trend in the tropical land evapotranspiration (Fig. 3) might be related to the change in soil water content. Under the high emission scenario of SSP585, more than half of the earth's land surface is likely to experience a severe limitation in future soil water content[35], which would exert an inhibitory effect on the tropical land evapotranspiration, as is supported by the positive correlation between the soil water content and evapotranspiration in Supplementary Fig. 12. If this kind of mechanism overwhelms the positive effect of LAI growth, decrease in evapotranspiration can be expected.

DISCUSSION
We define the wet and dry seasons over the tropical land surface as May to July and January to March, respectively, in this study. We

first exclude the subareas different from the whole tropical land area in which dry-season months are defined as May to July. These subareas are rain-less and desert regions. EC method is then applied to the remaining area and the constrained result is found to be quite similar to that of the whole tropical land area, with the discrepancy of merely 14.5–19.3% (Supplementary Fig. 13). We then establish emergent relationships between historical monthly dT/dP and future annual dT/dP, as in Thackeray et al.[37], and find that the relationships are most significant for the defined dry-season months (i.e. May to Jul.) (Supplementary Fig. 14), which also leads to the largest uncertainty reductions for the constrained future annual dT/dP.

We use historical dry season dT/dP to constrain the future annual dT/dP over the tropical land. We contend the plausible mechanism underpinning this emergent relationship is related to the evaporative cooling effect: increased precipitation leads to more water availability on the ground and in the soil, enhancing the cooling effect of evapotranspiration on sensible heating, and subsequently lowering the temperature of the tropical land surface, leading to a negative value of dT/dP[1,2,29]. This is supported by the antiphase oscillation between annual mean evapotranspiration and temperature over the tropical land (Fig. 1c, Supplementary Fig. 3). A model with a high evaporative cooling effect tends to produce a more negative dT/dP in both the
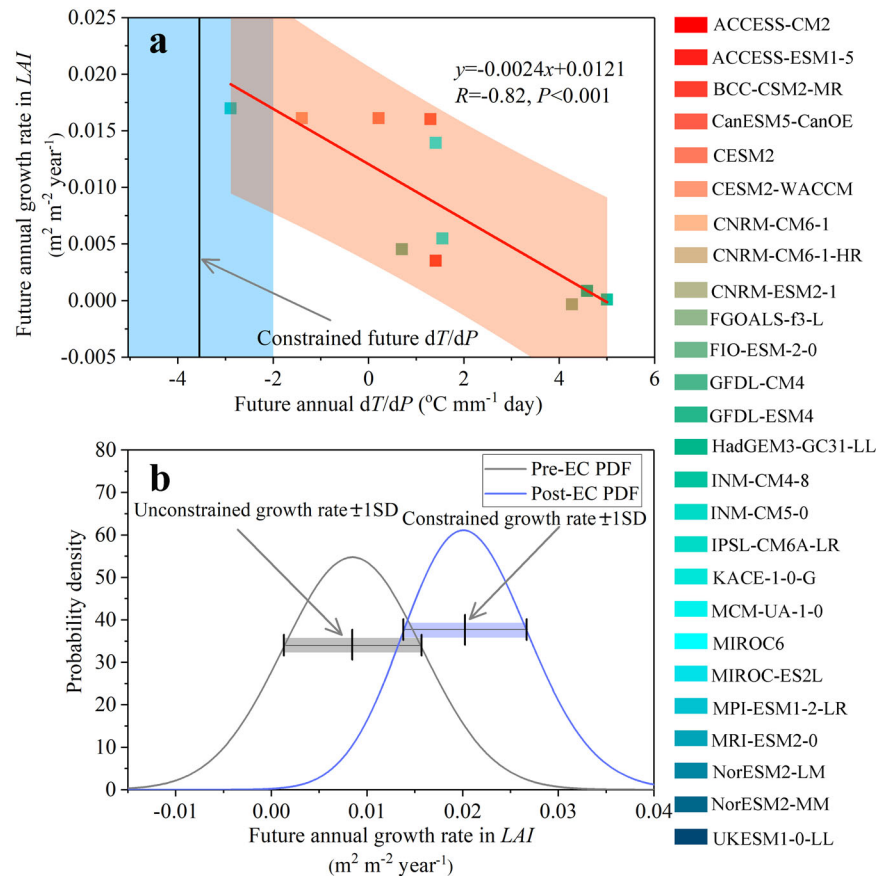
Fig. 4 EC on future annual growth rate in tropical land LAI based on CMIP6 models (see Supplementary Table 1) under the SSP585 scenario. a The constraint consists of a linear regression (with the associated forecast error) between the future annual dT/dP and future annual growth rates in tropical land LAI (red line and orange shaded area); the constrained data is computed by projecting the constrained future annual dT/dP ± one standard deviation (SD, vertical black line ± light blue rectangle) onto the regression. **b** Blue and gray lines are PDFs for the constrained (post-EC) and unconstrained (pre-EC) future annual growth rates in tropical land LAI.

historical and future periods, and vice versa. The inter-model spread in both the historical dry season dT/dP and the future annual dT/dP are dependent on the same evaporative cooling mechanism, which supports the existence of an emergent relationship between them. As noted by Hall et al. (2019)[10], verification of the mechanism underpinning the emergent relationship is most straightforward and effective when the same physical feedback process involves both the predictor and the predictand, and the only difference is the time scale over which the process occurs. Hence, an emergent constraint that focuses on the projection of a variable onto itself (i.e. the historical dry season dT/dP onto the future annual dT/dP in our case) is most straightforward and reliable.

In Fig. 2b, there is a striking change in dT/dP (i.e. 1.03 °C mm^{-1} day to −3.52 °C mm^{-1} day) after applying the EC method. From Fig. 2a, we see that modeled results of both historical dry season dT/dP and future annual dT/dP show a large spread across the 26 CMIP6 models, rather than biases from individual models, and the collection of data points forms the emergent relationship. If we eliminate the handful of models with negative values of future annual dT/dP, the emergent relationship still exists and changes little. The major driving factor for the significant shift in the future annual dT/dP from pre-EC to post-EC conditions is the observed historical dry season dT/dP (black vertical line), which is smaller than all the modeled values and results in the strongly negative value of future annual dT/dP when substituting the observation into the emergent relationship (i.e. the red regression line in Fig. 2a). This in turn highlights the high uncertainty of the CMIP model

simulations and the efficiency of the EC method. We can also see from Supplementary Table 2 that the observed historical dry season dT/dP values of the four datasets and the corresponding post-EC future annual dT/dP are all negative, and the changes from pre-EC to post-EC results are comparable with the result shown in Fig. 2, further supporting the method and conclusions of our study.

The Amazonian forest loss is projected to cross a tipping point and becomes increasingly severe as future annual ΔT/ΔP decreases[12], whereas the tropical LAI growth rate in this study experiences an obvious increase as future annual dT/dP declines (Fig. 4). This divergent behavior can be explained by different climate characteristics in these two regions. In the Amazon, precipitation is abundant and has experienced a limited decrease (see Fig. 1a in Chai et al.[12]); more negative dT/dP indicates more temperature warming, which is unfavorable for vegetation growth due to limitations in water use efficiency, photosynthesis and CO_2 fertilization[12,18–24]. This demonstrates that the Amazonian forest cover is mainly controlled by temperature. Nevertheless, the whole tropical land surface, assessed in this work, contains a wide variety of subareas, including both arid deserts and humid rainforests, where precipitation and temperature have respectively witnessed obvious decreases and increases (see Fig. 1a in this study). Over this broader area, a more negative dT/dP (namely the more negative linear regression slope in Fig. 1b in this study) means a lesser decrease in precipitation for a given increase in temperature (it can be seen from Fig. 1a that the increasing rate in temperature is roughly stable after 1975 whereas the decreasing

rate in precipitation slowed from 1975–1992 to 1992–2005), which is favorable for vegetation growth due to higher water availability[12,18–20,22–24]. Recognition of the key environmental variables driving the two different spatial-scale vegetation greenings is quite instructive for ecological preservation.

Apart from future annual dT/dP, we find that the historical LAI change also has a significant emergent relationship with the future LAI trend across CMIP6 models (Supplementary Fig. 15a). After combining this EC with the observation of LAI (0.0069 m^2 m^{-2} yr^{-1}), we estimate that the constrained future annual growth rate in LAI is most likely to reach 0.0192 m^2 m^{-2} yr^{-1}, which is quite consistent with the result (0.0205 m^2 m^{-2} yr^{-1}) obtained by using the constrained future annual dT/dP, with a discrepancy is only of 6.3%. These two equivalent results further improve the reliability of the finding in this study. In contrast, historical changes of evapotranspiration, temperature and precipitation show insignificant relationships with future LAI and evapotranspiration variations (Supplementary Fig. 15b–f).

Existing emergent constraint-based findings[13,37–42] are uniformly based on the assumption of the same plausible mechanism underpinning the inter-model spreads in both the historical and future changes for a certain environmental variable. This is the reason why all the previous studies[11,37,38,43] use a linear emergent relationship to reduce the prediction uncertainty in future variables. Similarly, in this study, our emergent constraint focuses on the projection of a variable onto itself (i.e. the historical dT/dP onto the future dT/dP), which involves in the same physical mechanism for both the predictor and the predictand. Thus, a linear emergent relationship is a more reasonable selection.

One limitation of this study is related to the uncertainty of the observational datasets. Different datasets exhibit a discrepancy in estimating the observed dT/dP, which may affect the post-EC results. Considering a range of observational datasets might be an effective way to relieve this influence. Here, we adopt four widely used datasets and find that the pre-EC dT/dP values are the same under a given SSP scenario, the post-EC dT/dP values are consistently negative, and the negative post-EC dT/dP values are comparable under a given SSP scenario (Supplementary Table 2), which confirms the reliability of our findings. Furthermore, another synthetic method, termed the Hierarchical Emergent Constraint (HEC) framework[44], also provides a practical pattern for constraining the future climate projections, given that it incorporates the present-future climate correlation, the bias between observations and ensemble mean, and the observation uncertainty. After using this method, we find that the constrained future annual dT/dP remains virtually unchanged (i.e. -0.98 °C mm^{-1} day under SSP126, −1.49 °C mm^{-1} day under SSP245, −2.51 °C mm^{-1} day under SSP370 and −3.05 °C mm^{-1} day under SSP585) compared with the results seen in Supplementary Table 2 (i.e. −1.10 °C mm^{-1} day under SSP126, −1.63 °C mm^{-1} day under SSP245, −2.86 °C mm^{-1} day under SSP370 and −3.52 °C mm^{-1} day under SSP585), with a discrepancy of merely 8.6–13.4%, which further improves the reliability of our main findings.

METHODS

Average values
Values of temperature, precipitation, evapotranspiration and LAI are taken directly from the relevant datasets (see Data Availability). All values are at the grid scale, bounded in the geographic land area within 23.5°S–23.5°N and 180°W–180°E. Spatial averages are obtained over the tropical land area. Herein, dT/dP is the rate of change of tropical land-surface average temperature with respect to tropical land-surface average precipitation. Changes in evapotranspiration and LAI are also derived from corresponding spatial averages.

Linear regression and forecast error
A linear regression is performed between x (independent variable) and y (dependent variable) using the least squares method[6]. That is, the best fit line corresponds to the minimum quadratic sum of the normal distances between the data points and the fitted line. Then, the best-estimate value of y (y_p) for a given value of x (x_p) is obtained by substituting x_p into the regression equation of the fit line[6,12,13].

The forecast error of y_p at x_p is estimated as

$$\sigma(y_p) = s\sqrt{1 + \frac{1}{N} + \frac{(x_p - \overline{x})^2}{N \cdot \sigma_x^2}} \tag{1}$$

where N is the number of samples, $\overline{x}$ is the geometric average across all elements in the independent variable sample, σ_x is the variance of x, and s is used to minimize the quadratic sum of the vertical distances during the linear regression analysis. σ_x and s are respectively calculated as follows:

$$\sigma_x = \sqrt{\sum_{i=1}^{N}(x_i - \overline{x})^2} \tag{2}$$

$$s^2 = \min\left(\frac{1}{N-2}\sum_{i=1}^{N}(y_{pi} - y_i)^2\right) \tag{3}$$

where x_i and y_i are the ith elements in samples of the independent and dependent variables, and y_{pi} is the value of y_p on the best fit line corresponding to y_i.

In Figs. 2a, 3a, 4a, and Supplementary Fig. 7a, c, e and 10a, x represents the historical dry season dT/dP and future annual dT/dP, respectively, and y represents future annual dT/dP, future change in tropical land evapotranspiration, and future annual growth rate in tropical land LAI, separately. Meanwhile, the observed dry season average dT/dP (vertical black line) ± one standard deviation (light blue rectangle) in Fig. 2a and Supplementary Fig. 7a, c, e and 10a are also determined using a linear regression process, in which the best estimate (i.e. the vertical black line) is the slope of the linear regression line between observed historical dry season T and observed historical dry season P, and a single standard deviation (i.e. the light blue rectangle) is calculated by Eq. (1). Subsequently, the constrained future annual dT/dP (vertical black line) ± one standard deviation (light blue rectangle) in Figs. 3a, 4a are obtained by projecting the best estimate of historical dry season dT/dP onto the red regression line and the orange shaded area in Fig. 2a.

PDFs
Following Cox et al.[6] and Chai et al.[12], PDFs of pre-EC values of dependent variables are directly calculated from

$$P(y) = \frac{1}{\sqrt{2\pi\sigma(y_p)^2}}\exp\left[-\frac{(y - y_p)^2}{2\sigma(y_p)^2}\right] \tag{4}$$

By comparison, post-EC values (y') are constrained by dataset observations, and the corresponding PDFs are determined from

$$P(y') = \int_{-\infty}^{+\infty} P(y)P(x')dx' \tag{5}$$

where x' represents the independent variable derived from observed datasets rather than the model results.

Hierarchical emergent constraint (HEC) framework
The hierarchical emergent constraint method requires data for the projected future climate variable (y), alongside simulated and observed current climate variables (x and x_o). Least-squares linear

regression is applied to establish the emergent relationship between x and y:

$$y = k(x - \overline{x}) + \overline{y} \tag{6}$$

where k is the regression coefficient, which can be calculated by using Eq. (7); $\overline{x}$ and $\overline{y}$ are the model ensemble mean values of x and y.

$$k = \rho \frac{\sigma_y}{\sigma_x} \tag{7}$$

where ρ is the correlation coefficient between x and y, and σ_x and σ_y are standard deviations of x and y across the CMIP6 models.

If the emergent relationship is causal and significant, we can constrain y by combining with the observed current climate variable x_o and its uncertainty. Assuming that the observation is related to the current climate through an additive-noise model under Gaussian assumptions, we use the signal-noise ratio (SNR) in x_0 to correct the scaling factor k (Eq. (8)). SNR defines the relative strength of the signal variability to the noise variability and is estimated by using Eq. (9), where σ_x^2 and σ_o^2 are variances across the models and across the different observation datasets. If the noise dominates the signal, the forecast anomaly will approach 0. Otherwise, if the signal drives the noise (i.e. SNR ≥ 1), the correction through Eq. (8) has little effect, and thus the constrained future climate $\overline{y_0}$ with its standard deviation can be estimated by Eqs. (10) and (11), respectively.

$$k^* = \frac{1}{1 + \text{SNR}^{-1}} k \tag{8}$$

$$\text{SNR} = \frac{\sigma_x^2}{\sigma_0^2} \tag{9}$$

$$\overline{y_0} = \overline{y} + \frac{k}{1 + \text{SNR}^{-1}} (\overline{x_0} - \overline{x}) \tag{10}$$

$$\sigma_y^2 = \left(1 - \frac{\rho^2}{1 + \text{SNR}^{-1}}\right) \sigma_y^2 \tag{11}$$

After using the HEC framework, the uncertainty of the projected future climate y_0 is reduced by $\frac{\rho^2}{1 + \text{SNR}^{-1}}$. More detailed information of the HEC framework can be seen in Bowman et al.[44].

DATA AVAILABILITY
CMIP6 model simulations of monthly data of temperature/precipitation during 1949–2100, and evapotranspiration and LAI during 2015–2100 under the emission scenarios of SSP126, SSP245, SSP370 and SSP585 were collected from https://esgf-node.llnl.gov/projects/cmip6/. Observed monthly temperature and precipitation data during 1949–2005 are derived from HadCRUT4 (http://www.cru.uea.ac.uk/), GPCC (https://climatedataguide.ucar.edu/climate-data/gpcc-global-precipitation-climatology-centre), NOAA (https://www.esrl.noaa.gov/psd/data/gridded/data.noaaglobaltemp.html), GISS (https://www.esrl.noaa.gov/psd/data/gridded/data.gistemp.html) and Delaware (https://psl.noaa.gov/data/gridded/data.UDel_AirT_Precip.html) datasets. HadCRUT4 and Delaware provide both temperature and precipitation data, whereas the GPCC dataset solely provides precipitation data, and NOAA and GISS datasets only provide temperature data. Hence, we use HadCRUT4, Delaware, and combinations of GISS + GPCC and NOAA + GPCC to establish the sensitivity of tropical land-surface temperature to precipitation in this study. Observed monthly data of evapotranspiration during 1980–2014 were gathered from the GLEAM dataset (https://www.gleam.eu/).

CODE AVAILABILITY
The code used to generate the results for this study is available upon reasonable request from the corresponding author.

REFERENCES
1. Trenberth, K. E. & Shea, D. J. Relationships between precipitation and surface temperature. *Geophys. Res. Lett.* **32**, L14703 (2005).
2. Adler, R. F. et al. Relationships between global precipitation and surface temperature on interannual and longer timescales (1979-2006). *J. Geophys. Res.—Atmos.* **113**, D22104 (2008).
3. Wang, J. J., Adler, R. F. & Gu, G. J. Tropical rainfall-surface temperature relations using Tropical Rainfall Measuring Mission precipitation data. *J. Geophys. Res.—Atmos.* **113**, D18115 (2008).
4. Frierson, D. M. W. et al. Contribution of ocean overturning circulation to tropical rainfall peak in the Northern Hemisphere. *Nat. Geosci.* **6**, 940–944 (2013).
5. Laine, A., Nakamura, H., Nishii, K. & Miyasaka, T. A diagnostic study of future evaporation changes projected in CMIP5 climate models. *Clim. Dyn.* **42**, 2745–2761 (2014).
6. Cox, P. M., Huntingford, C. & Williamson, M. S. Emergent constraint on equilibrium climate sensitivity from global temperature variability. *Nature* **553**, 319–322 (2018).
7. Jimenez-de-la-Cuesta, D. & Mauritsen, T. Emergent constraints on Earth's transient and equilibrium response to doubled CO_2 from post-1970s global warming. *Nat. Geosci.* **12**, 902–905 (2019).
8. Feron, S., Cordero, R. R., Damiani, A. & Jackson, R. B. Climate change extremes and photovoltaic power output. *Nat. Sustain.* **4**, 270–276 (2021).
9. Taylor, K. E., Stouffer, R. J. & Meehl, G. A. An overview of CMIP5 and the experiment design. *Bull. Am. Meteorol. Soc.* **93**, 485–498 (2012).
10. Hall, A., Cox, P., Huntingford, C. & Klein, S. Progressing emergent constraints on future climate change. *Nat. Clim. Change* **9**, 269–278 (2019).
11. Chai, Y. F. et al. Constrained CMIP6 projections indicate less warming and a slower increase in water availability across Asia. *Nat. Commun.* **13**, 4124 (2022).
12. Chai, Y. F. et al. Constraining Amazonian land surface temperature sensitivity to precipitation and the probability of forest dieback. *npj Clim. Atmos. Sci.* **4**, 6 (2021).
13. Shiogama, H., Watanabe, M., Kim, H. & Hirota, N. Emergent constraints on future precipitation changes. *Nature* **602**, 612–616 (2022).
14. Chai, Y. F. et al. Using precipitation sensitivity to temperature to adjust projected global runoff. *Environ. Res Lett.* **16**, 124032 (2021).
15. Papalexiou, S. M., Rajulapati, C. R., Clark, M. P. & Lehner, F. Robustness of CMIP6 historical global mean temperature simulations: Trends, long-term persistence, autocorrelation, and distributional shape. *Earth's Future* **8**, e2020EF001667 (2020).
16. Wang, Z. Z., Zhan, C. S., Ning, L. K. & Guo, H. Evaluation of global terrestrial evapotranspiration in CMIP6 models. *Theor. Appl. Climatol.* **143**, 521–531 (2021).
17. Zhu, Y. Y. & Yang, S. N. Interdecadal and interannual evolution characteristics of the global surface precipitation anomaly shown by CMIP5 and CMIP6 models. *Int. J. Climatol.* **41**, E1100–E1118 (2021).
18. Cox, P. M. et al. Amazonian forest dieback under climate-carbon cycle projections for the 21st century. *Theor. Appl. Climatol.* **78**, 137–156 (2004).
19. Imbach, P. et al. Modeling potential equilibrium states of vegetation and terrestrial water cycle of Mesoamerica under climate change scenarios. *J. Hydrometeorol.* **13**, 665–680 (2012).
20. Drijfhout, S. et al. Catalogue of abrupt shifts in Intergovernmental Panel on Climate Change climate models. *Proc. Natl Acad. Sci. USA* **112**, E5777–E5786 (2015).
21. Cox, P. M. et al. Sensitivity of tropical carbon to climate change constrained by carbon dioxide variability. *Nature* **494**, 341–344 (2013).
22. Alemayehu, T., van Griensven, A., Woldegiorgis, B. T. & Bauwens, W. An improved SWAT vegetation growth module and its evaluation for four tropical ecosystems. *Hydrol. Earth Syst. Sci.* **21**, 4449–4467 (2017).
23. Berg, A. & Sheffield, J. Evapotranspiration partitioning in CMIP5 models: uncertainties and future projections. *J. Clim.* **32**, 2653–2671 (2019).
24. Mendivelso, H. A., Camarero, J. J., Gutierrez, E. & Castano-Naranjo, A. Climatic influences on leaf phenology, xylogenesis and radial stem changes at hourly to monthly scales in two tropical dry forests. *Agr. For. Meteorol.* **216**, 20–36 (2016).
25. Li, B. G. et al. The contribution of china's emissions to global climate forcing. *Nature* **531**, 357–361 (2016).
26. Tokarska, K. B. & Gillett, N. P. Cumulative carbon emissions budgets consistent with 1.5 degrees C global warming. *Nat. Clim. Change* **8**, 296–299 (2018).
27. Tong, D. et al. Committed emissions from existing energy infrastructure jeopardize 1.5 degrees C climate target. *Nature* **572**, 373–377 (2019).
28. Fernandez-Martinez, M. et al. Global trends in carbon sinks and their relationships with CO_2 and temperature. *Nat. Clim. Change* **9**, 73–79 (2019).
29. Muller, C. J. & O'Gorman, P. A. An energetic perspective on the regional response of precipitation to climate change. *Nat. Clim. Change* **1**, 266–271 (2011).
30. Luo, X. Z. & Keenan, T. F. Tropical extreme droughts drive long-term increase in atmospheric CO_2 growth rate variability. *Nat. Commun.* **13**, 1193 (2022).
31. Le, T. & Bae, D. H. Response of global evaporation to major climate modes in historical and future Coupled Model Intercomparison Project Phase 5 simulations. *Hydrol. Earth Syst. Sci.* **24**, 1131–1143 (2020).

32. Le, T. & Bae, D. H. Causal impacts of El Nino-Southern oscillation on global soil moisture over the period 2015-2100. *Earth's Future* **10**, e2021EF002522 (2022).

33. Easterling, D. R. et al. Climate extremes: observations, modeling, and impacts. *Science* **289**, 2068–2074 (2000).

34. Chen, X., Alimohammadi, N. & Wang, D. B. Modeling interannual variability of seasonal evaporation and storage change based on the extended Budyko framework. *Water Resour. Res.* **49**, 6067–6078 (2013).

35. Cook, B. I. et al. Twenty-first century drought projections in the CMIP6 forcing scenarios. *Earth's Future* **8**, UNSP e2019EF001461 (2020).

36. Jung, M. et al. Recent decline in the global land evapotranspiration trend due to limited moisture supply. *Nature* **467**, 951–954 (2010).

37. Thackeray, C. W. & Hall, A. An emergent constraint on future Arctic sea-ice albedo feedback. *Nat. Clim. Change* **9**, 972–978 (2019).

38. Hall, A. & Qu, X. Using the current seasonal cycle to constrain snow albedo feedback in future climate change. *Geophys. Res. Lett.* **33**, L03502 (2006).

39. Sherwood, S. C., Bony, S. & Dufresne, J. L. Spread in model climate sensitivity traced to atmospheric convective mixing. *Nature* **505**, 37–42 (2014).

40. DeAngelis, A. M., Qu, X., Zelinka, M. D. & Hall, A. An observational radiative constraint on hydrologic cycle intensification. *Nature* **528**, 249–253 (2015).

41. Wenzel, S., Cox, P. M., Eyring, V. & Friedlingstein, P. Projected land photosynthesis constrained by changes in the seasonal cycle of atmospheric CO_2. *Nature* **538**, 499–501 (2016).

42. Terhaar, J., Kwiatkowski, L. & Bopp, L. Emergent constraint on Arctic Ocean acidification in the twenty-first century. *Nature* **582**, 379–383 (2020).

43. Tokarska, K. B. et al. Past warming trend constrains future warming in CMIP6 models. *Sci. Adv.* **6**, eaaz9549 (2020).

44. Bowman, K. W., Cressie, N., Qu, X. & Hall, A. A hierarchical statistical framework for emergent constraints: Application to snow-albedo feedback. *Geophys. Res. Lett.* **45**, 13050–13059 (2018). (2018).

45. Lian, X. et al. Partitioning global land evapotranspiration using CMIP5 models constrained by observations. *Nat. Clim. Change* **8**, 640–646 (2018).

AUTHOR CONTRIBUTIONS

B.Y.Z. and Y.F.C. designed the research, led the writing and performed the data analysis; Y.Z.C., X.Y.H., W.R.B., A.G.L.B., and L.S. contributed to the structure and writing of each version of the manuscript.

COMPETING INTERESTS

The authors declare no competing interests.

ADDITIONAL INFORMATION

Supplementary information The online version contains supplementary material available at https://doi.org/10.1038/s41612-023-00419-x.

Correspondence and requests for materials should be addressed to Yuanfang Chai.

Reprints and permission information is available at http://www.nature.com/reprints

Publisher's note Springer Nature remains neutral with regard to jurisdictional claims in published maps and institutional affiliations.